Ultraviolet photodissociation action spectroscopy of the N-pyridinium cation

Christopher S. Hansen,[1,a)] Stephen J. Blanksby,[2] Nahid Chalyavi,[3] Evan J. Bieske,[3] Jeffrey R. Reimers,[4,5] and Adam J. Trevitt[1,b)]
[1]*School of Chemistry, University of Wollongong, NSW 2522, Australia*
[2]*Central Analytical Research Facility, Queensland University of Technology, QLD 4000, Australia*
[3]*School of Chemistry, The University of Melbourne, VIC 3010, Australia*
[4]*School of Physics and Materials Science, University of Technology Sydney, NSW 2007, Australia*
[5]*International Centre for Quantum and Molecular Structure, Shanghai University, Shanghai 200444, China*

(Received 27 October 2014; accepted 2 December 2014; published online 5 January 2015)

The $S_1 \leftarrow S_0$ electronic transition of the *N*-pyridinium ion ($C_5H_5NH^+$) is investigated using ultraviolet photodissociation (PD) spectroscopy of the bare ion and also the N_2-tagged complex. Gas-phase *N*-pyridinium ions photodissociate by the loss of molecular hydrogen (H_2) in the photon energy range 37 000–45 000 cm^{-1} with structurally diagnostic ion-molecule reactions identifying the 2-pyridinylium ion as the exclusive co-product. The photodissociation action spectra reveal vibronic details that, with the aid of electronic structure calculations, support the proposal that dissociation occurs through an intramolecular rearrangement on the ground electronic state following internal conversion. Quantum chemical calculations are used to analyze the measured spectra. Most of the vibronic features are attributed to progressions of totally symmetric ring deformation modes and out-of-plane modes active in the isomerization of the planar excited state towards the non-planar excited state global minimum. © *2015 AIP Publishing LLC.* [http://dx.doi.org/10.1063/1.4904267]

I. INTRODUCTION

The *N*-pyridinium ion ($C_5H_5NH^+$) is the archetype protonated aromatic nitrogen heterocycle. Aromatic nitrogen heterocycles are ubiquitous in nature as the building blocks of biomolecules including the nucleobases and certain amino acid residues. Because photochemistry underlies the function of many biomolecules and can initiate DNA damage and thus cause disease,[1,2] there is significant interest in the ultraviolet (UV) photochemistry of aromatic heterocycles relevant to biology.[3–5] It is postulated that the deactivation of excited DNA molecules may involve local, "monomer-like" processes[2] reinforcing the importance of understanding the photochemistry of the molecular subunits comprising larger biologically relevant compounds. As many amino acids may become protonated at physiologically relevant pH, and because hydrogen-bonding in the base-pairing process imposes a protonation effect onto the nitrogen atom, insight into the photochemistry of protonated nitrogen heterocycles aids in understanding biologically relevant photochemistry. Several recent studies demonstrate that characterizing the gas-phase quantum dynamics and photochemistry of isolated biomolecules provides insight into their condensed phase behaviour.[2,5–8]

Beyond Earth, protonated aromatic compounds are postulated to carry unassigned interstellar absorption bands and it has been suggested that aromatic nitrogen heterocycles are present within interstellar media.[9,10] Pyridine derivatives have been detected in meteorites[11,12] and may exist in extraterrestrial atmospheres.[13,14] It is also proposed that nitrogen heterocycles may have been involved in the chemical origin of life.[10,15]

Given the importance and relevance of protonated aromatic nitrogen heterocycles, it is perhaps surprising that many of the electronic, spectroscopic, and photochemical properties are not fully understood for the simplest molecule in this class, the *N*-pyridinium ion. Neutral (unprotonated) pyridine is planar and well characterized in its ground electronic state,[16–19] when excited to its lowest singlet $\pi^* \leftarrow \pi$ electronic state (S_2) the planar geometry is destabilized. Like many other small aromatics,[20–22] electronically excited pyridine can access a pathway towards a non-planar, prefulvenic valence isomer along a coordinate that ultimately couples to the ground electronic state.[17,23–25] This behaviour is a familiar feature in the deactivation of electronically excited aromatics and has been observed experimentally for pyridine.[17,23,26,27] While control over this transformation may have promising synthetic applications,[28] it presents a significant spectroscopic challenge. The rapid and efficient deactivation manifests in fluorescence quenching,[8,29–31] short excited state lifetimes, and lifetime-broadened absorption profiles.[17,23,32] Intersystem crossing (ISC) throughout the manifold of singlet and triplet states of both $\pi^* \leftarrow \pi$ and $\pi^* \leftarrow n$ character is also rapid in accordance with El-Sayed's rules.[17,30,33] Furthermore, additional complications arise due to the overlap of the two lowest $\pi^* \leftarrow n$ states (S_1 and S_3) and the S_2 $\pi^* \leftarrow \pi$ electronic band, congesting the absorption spectra.[16,17,32]

Protonation of pyridine minimally perturbs the π system while constraining the non-bonding nitrogen lone pair electrons to the covalent N–H bond. This removes the $\pi^* \leftarrow n$

a)Electronic mail: csh297@uowmail.edu.au
b)Electronic mail: adamt@uow.edu.au

states from the electronic manifold. Consequently, the first (and only low-lying) electronic transition ($S_1 \leftarrow S_0$) of the *N*-pyridinium ion is analogous to the $S_2 \leftarrow S_0$ transition in neutral pyridine and intersystem crossing to T_1 ($\pi^* \leftarrow \pi$) is now spin-orbit forbidden. It has been shown that, when compared to the S_2 state of neutral pyridine, the S_1 state of the *N*-pyridinium ion is subject to the same rapid and efficient excited state deactivation along a non-planar coordinate[17] and that the absorption spectrum is essentially unshifted.[17,32]

The positive charge afforded by protonation allows the *N*-pyridinium ion to be interrogated using mass spectrometry-based spectroscopy techniques such as photodissociation (PD) action spectroscopy and this is the focus of the current paper. A PD action spectrum of the *N*-pyridinium ion recorded using a Fourier-Transform Ion Cyclotron Resonance (FT-ICR) mass spectrometer and a series of diffuse light sources was recorded almost four decades ago.[32] This investigation revealed that gas-phase *N*-pyridinium photodissociates through the loss of molecular hydrogen (H_2) following UV excitation. The PD action spectrum obtained for this dissociation process exhibited a broad electronic band centered upon the vapor-phase S_2 band of neutral pyridine. However, this spectrum was recorded with a coarse wavelength increment and no vibronically resolved structure was observed.

In the present study, the photodissociation and spectroscopy of the *N*-pyridinium ion and its $C_5H_5ND^+$ (d_1) and $C_5D_5NH^+$ (d_5) isotopologues are investigated across the photon energy range 37 000–45 000 cm^{-1} (270–220 nm) using two different experimental arrangements. Consistent with previous studies, the dominant photoproduct is the loss of molecular hydrogen and the coproduct is investigated using structurally diagnostic ion-molecule reaction kinetics and electronic structure calculations, revealing the 2-pyridinylium ion as the exclusive coproduct (Fig. 1). The spectra recorded in this region reveal a broad electronic band exhibiting vibronically resolved structure. An electronic spectrum has also been recorded for *N*-pyridinium ions tagged with N_2 molecules that exhibit more cleanly resolved vibronic structure. These spectra are analyzed with the aid of comprehensive quantum chemical calculations through which it is shown that the excited state prefers a buckled, prefulvenic geometry. While totally symmetric ring-deformation modes prevail in the main progression, the spectrum is influenced by this non-planar distortion resulting in spectral fine structure, including a prominent low-frequency doublet, that is superimposed on the main progressions.

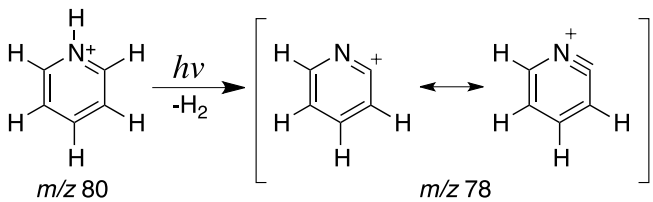

FIG. 1. The *N*-pyridinium ion photodissociates to form the 2-pyridinylium ion and molecular hydrogen following ultraviolet excitation in the region 37 000–45 000 cm^{-1} (270–220 nm).

II. EXPERIMENTAL METHODS

The electronic spectroscopy of the *N*-pyridinium cation was obtained using two different experimental strategies. The first instrument is located at the University of Wollongong and utilizes a commercial ion trap and a tunable UV laser to acquire PD mass spectra of ambient-temperature ions generated by electrospray ionization (ESI).[34] The second instrument, situated at The University of Melbourne, comprises a custom tandem mass spectrometer that generates and mass selects weakly bound pyridine–N_2 dimers, with N_2 serving as an inert tag molecule, that are irradiated by a counter-propagating tunable UV laser pulse.[35] Overviews of both instruments are given here, more detailed descriptions can be found in the aforementioned references.[34,35]

A. Ion trap photodissociation action spectroscopy

The first instrument is a linear quadrupole ion trap (QIT) mass spectrometer (Thermo Fisher Scientific LTQ) coupled to a tunable optical parametric oscillator (OPO) laser system (GWU-Lasertechnik flexiScan) pumped by the third harmonic (355 nm) of a 10 Hz, ~5 ns pulsewidth Nd:YAG laser (Spectra-Physics QuantaRay INDI). The linewidth of the OPO system is 4–11 cm^{-1} corresponding to a resolution limit of approximately 0.05 nm in the UV range of interest. $[M+H]^+$ or $[M+D]^+$ cations of pyridine (C_5H_5N) and d_5-pyridine (C_5D_5N) were generated by electrospray ionization of methanol (CH_3OH) or d_1-methanol (CH_3OD) solutions of the precursor. Ions in the QIT are expected to be thermalized to near-ambient temperature (307 ± 1 K)[36] through collisions with the helium buffer gas (2.5×10^{-3} Torr). The target ion *m/z* is then isolated with all other ions ejected. A single laser pulse from the tuneable OPO irradiates the trapped ions along the principal axis of the ion trap. Ions are then scanned out of the QIT and detected to record a photodissociation mass spectrum. A photodissociation yield is calculated as the ratio of the photoproduct peak (or peaks) area to the total ion count (TIC). The OPO is then stepped to the next wavelength ($\Delta\lambda = 0.1$ nm) and the process repeated. The photoproduct yield is plotted as a function of wavelength to construct the photodissociation action spectrum. The PD action spectra reported here are the average of three complete spectra using a wavelength step size of 0.1 nm with ~80 mass spectra (30 s of acquisition time) averaged at each wavelength.

Reagent grade pyridine (min. 99%) and HPLC grade methanol (min. 99.7%) were purchased from Thermo Fisher Scientific. Methanol-d_1 and pyridine-d_5 (both 99.5 atom % D) were purchased from Cambridge Isotope Laboratories (Andover, MA).

B. Resonance-enhanced photodissociation spectroscopy

The second instrument is a custom-built tandem mass spectrometer that couples to a tunable OPO laser system (Opotek Vibrant, line-width of ~5 cm^{-1}). Gas-phase pyridinium-N_2 complexes were prepared by seeding pyridine into a supersonic expansion of a N_2/H_2 gas mixture subjected

to electron bombardment. N_2 was chosen as a tag molecule rather than the more inert argon atom as the pyridinium ion ($C_5H_5NH^+$) is isobaric with Ar_2^+ ($m/z = 80$). The target ion complex was mass-selected by a quadrupole mass filter and deflected by a 90° quadrupole bender into an octopole ion guide. Here, the $C_5H_5NH^+$-N_2 ions were irradiated with the counter-propagating light pulse from the OPO. When the photon energy was resonant with a vibronic transition of the complex, the weak non-covalent pyridinium-N_2 bond was severed to yield the bare pyridinium ion and the neutral N_2 molecule. Following irradiation, the ions pass through a second quadrupole mass filter tuned to pass the bare pyridinium ion ($m/z = 80$) to the ion detector. This measurement is repeated at each wavelength. The resulting spectrum reports the photofragment signal as a function of wavelength. Because the weak pyridinium-N_2 intermolecular bond is broken when the dimer possesses excess thermal energy, and because the interaction between the pyridinium ion and the N_2 molecule is relatively weak, the spectra acquired using this instrument should approximate the absorption spectrum of the cold pyridinium ion, although the bands will be shifted due to the attached N_2 molecule. It is shown in Sec. IV B that the N_2 tag has a minor effect on the spectrum and photochemistry of the pyridinium ions.

III. COMPUTATIONAL METHODS

A. Franck-Condon (FC) analysis using Cartesian coordinates and complete-active-space self-consistent-field (CASSCF) electronic-structures

CASSCF[37–42] electronic-structure calculations were performed using the Gaussian 09[43] suite. In each case, a Dunning-type[44] augmented[45,46] correlation-consistent polarized valence double-ζ (aug-cc-pVDZ) basis set was used with an active space comprising the six valence π orbitals (3 occupied, 3 unoccupied) and 6 active electrons. PGOPHER[47] 7.1 was used to simulate vibronic FC absorption spectra from the CASSCF geometries and normal modes. The Wilson numbering convention for the normal modes of benzene is used to describe the in-plane skeletal ring deformation modes of the *N*-pyridinium ion.

B. Franck-Condon analysis using internal coordinates and time-dependent density functional theory (TD-DFT) electronic-structures

Gaussian 09(c01)[43] was used to perform TD-DFT[48–54] electronic structure calculations using the aug-cc-pVDZ basis set[44–46] and the CAM-B3LYP[55] functional: a long range-corrected version of the B3LYP hybrid functional. Because the nuclear displacements between electronic states were large, the normal mode analysis was conducted in redundant internal coordinates employing a procedure described elsewhere.[56] Briefly, the force constant (Hessian) matrix was read in from the Gaussian 09 log file using a custom FORTRAN program. The normal modes were transformed to orthonormal internal coordinates and the Duschinsky rotation matrices were calculated using the formalism of Reimers.[56] The structures of a symmetry-enforced, planar excited state, and the ring-buckled global minimum were projected onto the b_1 normal modes of the former. A potential energy surface was then constructed by the curvilinear interpolation between the two structures. The eigenvectors were calculated using harmonic normal mode analysis with a perturbation theory anharmonicity correction and the effective harmonic frequency of the ground electronic state was determined by calculating the Duschinsky matrix (in rectilinear coordinates) between the planar excited state and ground state and multiplying it by the b_1 displacement vector. As the displacements had been transformed into a normal mode basis, they were used to directly calculate vibrational overlap integrals and Franck-Condon factors from which transition electric dipole moments were calculated and the spectrum simulated.

C. Energy calculations

The energy scheme of the ground state dissociation process was generated using zero point energy (ZPE)-corrected energies computed using the Complete Basis Set (CBS)-QB3 CBS method[57–64] within the Gaussian 09 software.[43]

IV. RESULTS AND DISCUSSION

A. Photodissociation mass spectrometry and action spectroscopy (Wollongong experiment)

The PD action spectrum of the pyridinium cation ($C_5H_5NH^+$) was constructed from PD mass spectra acquired across the photon energy range 37 000–45 000 cm^{-1} (270–220 nm). To assist with spectral assignments, equivalent PD action spectra were also acquired for the $C_5H_5ND^+$ (d_1) and $C_5D_5NH^+$ (d_5) isotopologues. Representative PD mass spectra, acquired using a photon energy of $\lambda = 250$ nm, are presented in Fig. 2.

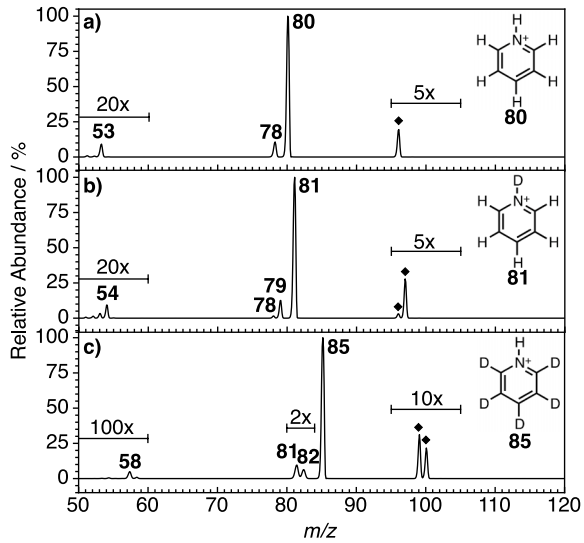

FIG. 2. Photodissociation mass spectra (λ = 250 nm) of the three *N*-pyridinium isotopologues: (a) $C_5H_5NH^+$, (b) $C_5H_5ND^+$, and (c) $C_5D_5NH^+$. The black diamonds indicate ions resulting from the addition of water (18 Da) to the photoproducts.

The dominant photodissociation pathway is the even-electron loss of molecular hydrogen as either H_2, HD, or D_2 according to the deuteration of the precursor cation. As reported by Freiser and Beauchamp,[32] unlabelled pyridinium ($m/z = 80$) photodissociates by H_2 loss to form a photoproduct ion at $m/z = 78$ (Fig. 2(a)). In this study, the $m/z = 78$ photoproduct ion population was identified as exclusively the 2-pyridinylium isomer by structurally diagnostic ion/molecule reaction kinetics (described in the supplementary material,[65] Sec. 3). Singly deuterated pyridinium ($m/z = 81$) loses both HD and H_2 to yield photoproduct ions at $m/z = 78$ and 79 (in a 1:8 ratio) following ultraviolet excitation (Fig. 2(b)) whereas d_5 pyridinium ($m/z = 85$) loses HD and D_2 to yield $m/z = 82$ and 81 photoproduct ions in a 2:3 ratio (Fig. 2(c)). The distribution of photoproduct isotopologues in Fig. 2 is likely to be affected by intramolecular hydrogen/deuterium (H/D) scrambling following excitation and preceding photodissociation. H/D scrambling is a familiar feature of aromatic photoactivation, often occurring on a microsecond timescale.[66,67] Minor peaks corresponding to the addition of background water occur 18 Da higher in mass than the dominant photoproduct and are labelled with black diamonds. These water addition signals scale linearly with the photoproduct signals and the action spectra reported herein include these peaks in the calculation of PD yields. There is also evidence for a minor photodissociation channel consistent with the loss of HCN (27 Da); the magnified peak corresponding to these ions at $m/z = 53$, 54, and 58 in Fig. 2(a), Fig. 2(b), and Fig. 2(c), respectively. This minor peak was not included in the calculation of PD yields for construction of PD action spectra.

Photodissociation action spectra acquired across the photon energy range 37 000–45 000 cm^{-1} (270–220 nm) are presented for the pyridinium d_0 and d_1 isotopologues in Fig. 3(a) and Fig. 3(b), respectively. The spectra exhibit minor intensity differences but are generally similar. Both spectra contain a single, vibronically structured electronic band spanning the experimental photon energy range. These bands have an onset at around 37 500 cm^{-1} and exhibit a sharp feature, labelled A, at 38 530 cm^{-1} for *N*-pyridinium-d_0 and 38 560 cm^{-1} for the d_1 isotopologue. This feature is the first member of a doublet with the second member (labelled B) occurring at A + 90 cm^{-1}. The other intense feature is labelled C and occurs at A + 260 cm^{-1}. There is also a pronounced low-energy shoulder at A − 100 cm^{-1}, labelled D. This set of four features is repeated 515 cm^{-1} higher in energy. It is known from a previous study of the *N*-methylpyridinium ion[67] and from simulations presented later that this ~500 cm^{-1} spacing corresponds to one quantum of the ν_6 (Wilson notation) ring-deformation mode. These eight features (two sets of four peaks) are repeated at least four times at +965 cm^{-1} intervals and this is rationalized as a progression of the ν_1 ring-breathing mode with at least 5 sequential quanta resolved. No significant anharmonicity is measured at four quanta of excitation (the spacing between consecutive ν_1 excitations is included in the supplementary material,[65] Fig. S1).

The d_5 spectrum is included in the supplementary material[65] (Fig. S2) and also reveals a single electronic band, although noticeably redshifted and more congested. Most of the spectral features present in the d_0 and d_1 spectra persist, but are suppressed, particularly at the lower energy part of the spectrum. The assignments for the d_5 spectrum are less certain than for the d_0 and d_1 spectra. The d_5 PD action spectrum also exhibits a progression built upon the ν_1 mode, however, the frequency is reduced to about 930 cm^{-1}. The 90 cm^{-1} doublet (A) is clearly resolved for the first five $n\nu_1$ bands, however, the $n\nu_1 + 1\nu_6$ bands are poorly resolved. The doublet feature is resolved for the $1\nu_1 + 1\nu_6$ band and is indicated with a black triangle in Fig. S2. The decreased wavenumber of the progression-building mode is consistent with its assignment as ν_1—deuterating the ring increases the reduced mass of the deformation. The photodissociation process is discussed in more detail in Sec. IV D.

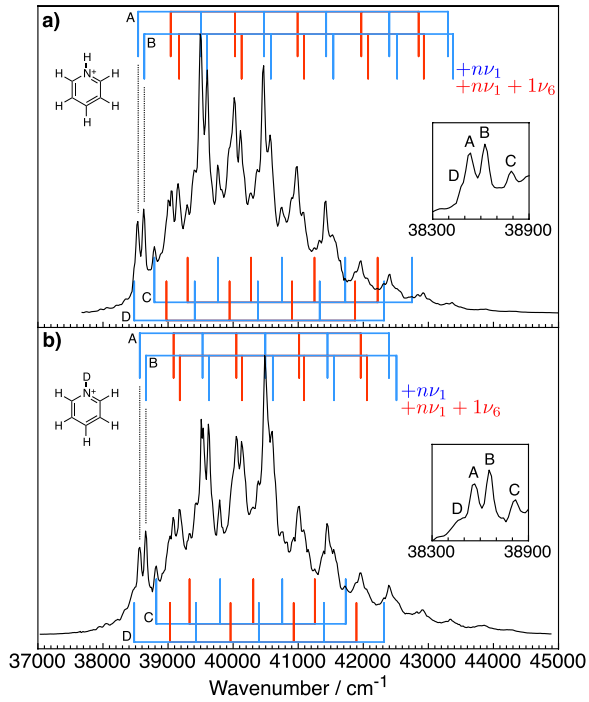

FIG. 3. Photodissociation action spectra of the (a) $C_5H_5NH^+$ and (b) $C_5H_5ND^+$ *N*-pyridinium isotopologues. The normalized yields of the photoproducts in Fig. 2 are plotted as a function of photon energy and vibrational progressions in the $^1B_2 \leftarrow {}^1A_1$ band are labelled. The insets show magnified portions of the spectrum around the first four unique spectral features.

To ensure that the observed widths of the spectral features were not limited by the OPO linewidth (4–11 cm^{-1}), a portion of the spectrum (39 000–39 800 cm^{-1}) was recorded using a dye laser with a linewidth of ~0.05 cm^{-1} (ca. 100x narrower). Details of the laser system and the measured spectra are included in the supplementary material[65] (Fig. S7). Spectra acquired using the OPO and the dye laser are almost identical with regard to peak positions, intensities, and bandwidths. Thus, the recorded spectrum reflects the properties of the trapped pyridinium ions and is not influenced by the linewidth of the photon source.

The PD action spectra in Fig. 3 are surprisingly detailed and the energy differences between many of the spectral features, e.g., B-A and A-D, are likely too low (<100 cm^{-1}) to be attributed to harmonic normal mode frequencies. To assist with the interpretation, complementary spectra were acquired

using resonance-enhanced photodissociation spectroscopy of N_2 tagged pyridinium ions.

B. Resonance-enhanced photodissociation of pyridinium-N_2 ions (Melbourne experiment)

Fig. 4(a) presents the resonance-enhanced photodissociation spectrum for the N_2-tagged d_0 pyridinium ion across the photon energy range 37 000–45 000 cm^{-1} (270–220 nm), the comparison to a simulated stick spectrum and assignments will be discussed later. When compared to the spectrum in Fig. 3(a), all of the previously identified features occur at almost the same photon energies. Importantly, this verifies that the closely spaced features in the tagged case are unlikely to be due to intermolecular modes. The N_2-tagged resonance-enhanced photodissociation spectrum is generally less congested and the onset is sharper than for the untagged species (Fig. 3(a)). Irradiation of the N_2-tagged species also results in $-[N_2+H_2]$ photoproducts, and the PD action spectrum for this channel is shown in Fig. 4(b). The details in this spectrum line up with the features in Fig. 4(a) but the intensity profile is closer to that of the untagged molecule in Fig. 3(a). The photodissociation yield (i.e., loss of H_2 or $[N_2+H_2]$) increases with photon energy for both the tagged and untagged species. The suppression of the doublet in the spectrum of the tagged complexes (Fig. 4) compared to the spectrum of untagged complexes (Fig. 3) is particularly notable. The presence of the neutral N_2 tag may subtly affect the Huang-Rhys factors (and thus the transition line strengths) of the states in the bending potential. It is expected that the neutral tag will have a minor effect on the band spacings and intensities but may lead to a uniform shift of the spectral features. The first intense feature ($A0_0^0$ in Fig. 4) occurs at 38 532 cm^{-1} in the spectra of the N_2-tagged complex and at 38 536 cm^{-1} in the spectra of the untagged ions (Fig. 3). This difference is less than the photon energy increment in this region (~15 cm^{-1}) and, within these experimental limitations, tagging a pyridinium ion with N_2 does not result in a significant bandshift.

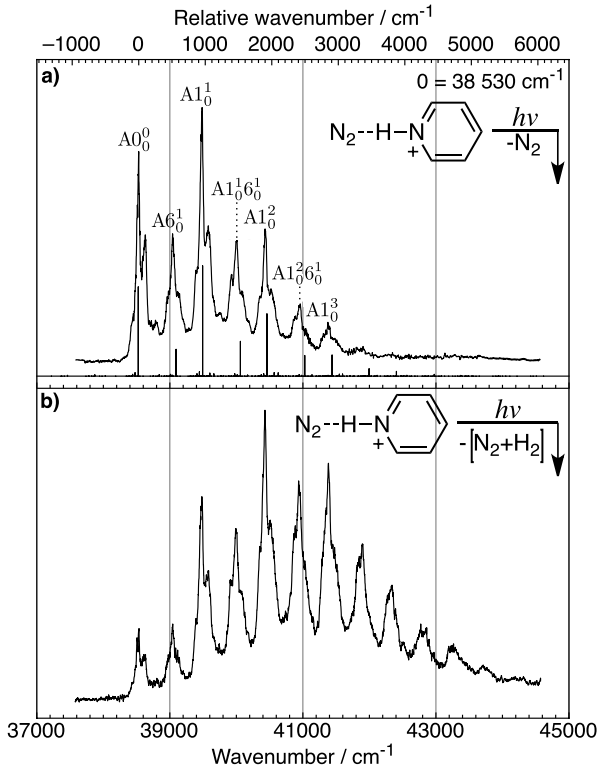

FIG. 4. (a) Electronic spectrum of the N_2-tagged *N*-pyridinium weakly bound dimer obtained by monitoring the yield of the bare ion following ultraviolet irradiation. The experimental spectrum is compared to a stick spectrum based on CASSCF(6,6)/aug-cc-pVDZ calculations and Franck-Condon simulations. (b) Photodissociation action spectrum of the N_2-tagged *N*-pyridinium complex monitoring the $-[N_2+H_2]$ channel.

C. Spectrum analysis

Two different approaches were used to simulate the vibronic absorption spectrum of the *N*-pyridinium ion and assign the main features. Both approaches are summarized briefly here and in detail in Subsections IV C 1 and IV C 2. The first was a conventional normal-mode analysis in Cartesian coordinates at planar geometries using the results of CASSCF electronic-structure calculations employing an active space comprising the six valence π orbitals (three occupied, three unoccupied). The second method for simulating the vibronic spectrum utilized TD-DFT electronic structures and a detailed normal-mode analysis in curvilinear coordinates and at non-planar geometries.

The PD action spectrum of the N_2-tagged *N*-pyridinium cation was presumed to correspond to the vibronic absorption spectrum. This is likely to be the case because loss of the weakly bound tag N_2 molecule should occur following either internal conversion (IC) from the S_1 state or fluorescence into ground state vibrational levels lying above the dissociation threshold. As is apparent from the spectra shown in Figs. 3 and 4(b), the intensities of the lower transitions are suppressed when PD spectra are recorded by monitoring channels involving loss of H_2.

1. Franck-Condon analysis using Cartesian coordinates and CASSCF electronic-structures

The electronic transition under consideration is of $\pi^* \leftarrow \pi$ character and is known, in the condensed phase, to populate the 1^1B_2 (C_{2v}) state,[16] which derives from the 1^1B_{2u} state in benzene. This band is a commonly observed feature in aromatic spectroscopy and appears at around 260 nm for most six-membered aromatics[68] and azabenzenes,[19] including neutral and protonated pyridine[17,32] and *N*-methylpyridinium.[67] Due to the $\pi^* \leftarrow \pi$ nature of the transition, and because all of the ion's valence electrons are constrained to covalent bonds, an active space made up of the six valence π orbitals (three occupied, three unoccupied) was chosen for the CASSCF calculations. In a recent study,[67] similar calculations on the *N*-methylpyridinium ion reproduced the main vibronic features present in the experimental PD action spectrum. The CASSCF(6,6)/aug-cc-pVDZ method predicts a stable planar S_1 excited state with an adiabatic excitation energy of 40 500 cm^{-1}, which is 2000 cm^{-1} above the first intense feature in the experimental spectrum. CASSCF energies are often higher than the experiment and this is commonly adjusted

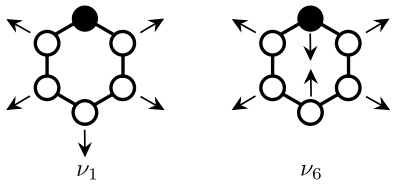

FIG. 5. Schematic representation of the totally symmetric (a_1) ν_1 and ν_6 modes (Wilson notation) of the *N*-pyridinium ion showing only the heavy nuclei (C and N). The arrows indicate the direction, but not the magnitude, of displacement.

by the inclusion of electron correlation through a perturbation theory correction to the MCSCF energy (e.g., CASPT2).

The room-temperature Franck-Condon absorption spectrum was simulated using the PGOPHER program.[47] Vibrational modes were successively included in the simulation in order of decreasing calculated FC activity, until the simulated spectrum was no longer significantly affected. Normal modes were restricted to 5 quanta of excitation in each electronic state. A total of four modes, all in-plane and totally symmetric (a_1) were included although the simulated spectrum is ultimately dominated by the two modes (ν_1 and ν_6) represented in Fig. 5. The simulated stick spectrum (based on the assigned "A" origin) is compared to the experimental resonance-enhanced photodissociation spectrum in Fig. 4(a); the calculated transitions are labelled above the profile of the experimental spectrum. This simulation supports the assignment of ν_1 as the progression building mode and ν_6 as responsible for the second set of four peaks. These two modes account for most of the intense vibronic structure, however, the doublet feature ("B" in Fig. 3), the low-energy shoulder ("D" in Fig. 3), and the additional feature at $A0_0^0 + 260$ cm^{-1} ("C" in Fig. 3) are not predicted by this simulation.

It will be shown in Sec. IV C 2 that the electronic excited-state minimum has a non-planar geometry, contrary to these CASSCF predictions. Nevertheless, they serve as a valuable starting point as they provide a bound excited state geometry that approximates the initially prepared Franck-Condon state. To understand the finer features of the spectrum, further analysis is needed.

2. Franck-Condon analysis using internal coordinates and TD-DFT electronic-structures

TD-DFT calculations employing the CAM-B3LYP functional and the aug-cc-pVDZ basis set predict a planar ground electronic state but a significantly non-planar S_1 excited state minimum. The buckled geometry of this optimized excited electronic state is included in the supplementary material[65] described in terms of Cartesian coordinates (Sec. 6) and is represented schematically in Fig. 6. This geometry involves significant pyramidalization of the nitrogen atom to a distance 0.64 Å out of the ring plane and a puckering of the ring such that the *para*-carbon is raised 0.13 Å above the ring plane. This valence isomer is reminiscent of prefulvenic isomers formed in the deactivation of other aromatics including benzene[21] and neutral pyridine[17] and it will be shown that this displacement, and the corresponding electronic potential

FIG. 6. Schematic representation of the *N*-pyridinium excited electronic state minimum structure as predicted by the CAM-B3LYP/aug-cc-pVDZ method. The annotated distances are the length of the vectors normal to the ring plane.

energy landscape, may be responsible for the unassigned fine structure in the experimental PD action spectra.

To approximate the "vertical" Franck-Condon excited state geometry, the minimum energy C_{2v} structure was calculated by optimizing the geometry of a C_{2v} symmetry-constrained excited state, leading to a second-order saddle point (Cartesian coordinates and normal modes included in the supplementary material,[65] Sec. 6) and a barrier to planarity of almost 2000 cm^{-1}. The potential energy curve for this isomerization, shown in Fig. 7, was constructed by interpolating between the optimized C_{2v} geometry and the non-planar, prefulvenic excited state minimum in modified curvilinear coordinates (described in the supplementary material,[65] Sec. 7). The reaction coordinate represents the minimum energy C_{2v} structure at 0% and the non-planar global minimum at 100%.

To construct an adiabatic potential energy surface that can be used to simulate the electronic spectrum, the reaction coordinate in Fig. 7 was first projected beyond the global minimum structure to $Q = Q_{C_{2v}} + 1.5(Q_{C_s} - Q_{C_{2v}})$. Where Q is a set of normal coordinates and $Q_{C_{2v}}$ and Q_{C_S} are the normal coordinates of the C_{2v} and global excited state minima, respectively. Because the potential curve is symmetric (a projection of −Q yields a pseudorotation of Q), the potential energy surface was reflected about the origin to construct the remaining half. The next step was to convert the length coordinate to a useful scale. As previously described in Sec. III B, the curvilinear displacement of the excited state from the C_{2v} minimum to the global minimum was projected onto the b_1 normal modes of the excited state C_{2v} minimum. The normal mode corresponding to nitrogen pyramidalization comprised 91% of the displacement and the ring-puckering mode made up 8%. The displacement vectors and contribution of

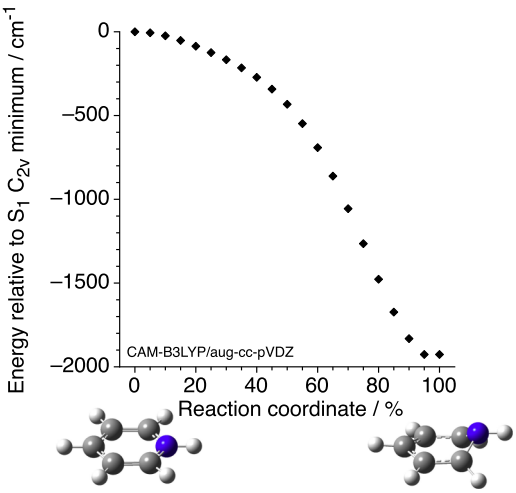

FIG. 7. Interpolated reaction coordinate for the isomerization of the electronically excited (S_1) *N*-pyridinium ion. The markers indicate single point energies calculated along the coordinate.

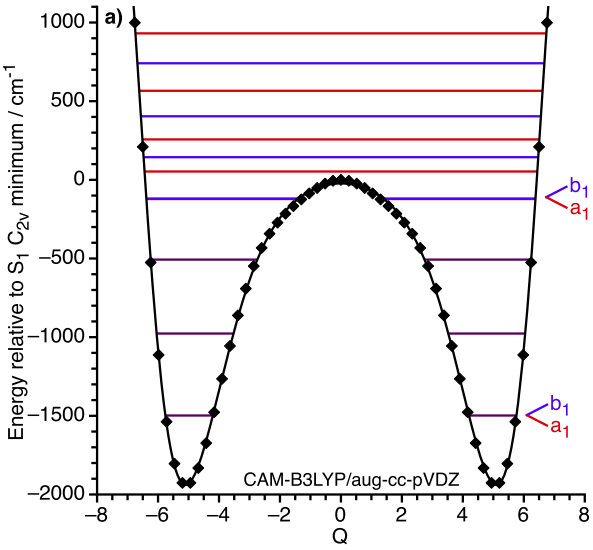

FIG. 8. Dimensionless, normal-mode projected, double-well potential energy surface of the first *N*-pyridinium excited electronic state.

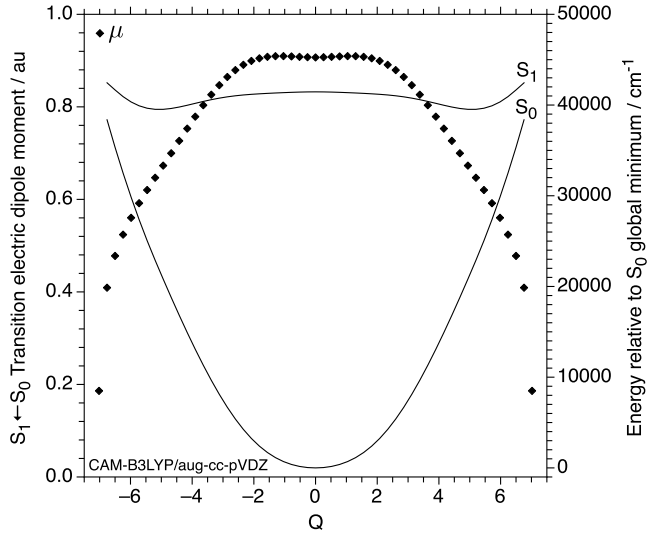

FIG. 9. Excited electronic state (S_1) dimensionless b_1 normal-mode projected displacement and (S_0) harmonic ground electronic state displacement (lines) overlaid with the CAM-B3LYP/aug-cc-pVDZ transition electric dipole moments (diamonds).

each b_1 normal mode are included in the supplementary material,[65] Table S1. Within this framework, the interpolated coordinate was rescaled to give the dimensionless normal-mode projection shown in Fig. 8.

To calculate the energy levels for the potential in Fig. 8, a single-exponential function was fitted to the data points where $|Q| > 5$, i.e., to the wall of the well. The potential energy surface was then extrapolated to a wall-height of 10^5 cm^{-1} and the entire potential was fitted by a 16th order polynomial. The vibrational wavefunctions were then expressed as a linear combination of 100 Hermite polynomial basis functions; the eigenvectors were found to be unchanged when 60 functions were used, thus confirming that the calculation had converged. The predicted pattern of energy levels is typical of a symmetric double-well potential energy curve; the energy levels occur in pairs—symmetric (red) and antisymmetric (blue) with respect to the coordinate Q—with the spacing between the levels of the pair increasing as the top of the barrier is approached.[69] In this case, the first three pairs of energy levels are essentially degenerate and the splitting only becomes discernible near the top of the well.

In order to simulate the absorption spectrum, the Duschinsky rotation matrix between the planar (C_{2v}) excited state and ground state minimum (included in the supplementary material,[65] Fig. S8) was calculated, in rectilinear coordinates, and used to rotate the b_1 displacement vector into the ground electronic state normal modes, from which the effective harmonic frequency of the ground state was calculated to be 627 cm^{-1}. Fig. 9 shows the adiabatic excited state surface and harmonic ground state overlaid with the TD-DFT transition electric dipole moments at each single point along the interpolation. It is apparent that the predicted transition probability is high about the top of the planarity barrier and that the states below the barrier are much less active in the absorption spectrum. This is perhaps unsurprising given the large geometry change but indicates significant breakdown of the Condon approximation [the transition moment can be considered the product of an electronic transition moment (μ) that is independent of nuclear coordinates and the square of a vibrational overlap integral (Franck-Condon factor)]. In this scenario, the true origin (0_0^0) transition is expected to be weak. As the displacements are defined in terms of normal modes, they can be used directly to evaluate vibrational overlap integrals and determine Huang-Rhys factors. Table I

TABLE I. Predicted energy levels of the b_1 normal-mode projected excited state displacement and the simulated transition electric dipole moments from a harmonic ground state. In bold are the transitions responsible for the four dominant predicted spectral features.

Energy[a]/cm^{-1}	Symmetry	$\|\mu\|^2$/au
−1498	a_1	0.0000
−1498	b_1	0.0000
−977	a_1	0.0000
−977	b_1	0.0000
−507	a_1	0.0002
−507	b_1	0.0000
−122	$\boldsymbol{a_1}$	**0.0348**
−119	b_1	0.0000
+53	$\boldsymbol{a_1}$	**0.6097**
+144	b_1	0.0000
+257	$\boldsymbol{a_1}$	**0.2280**
+404	b_1	0.0000
+566	$\boldsymbol{a_1}$	**0.0741**
+741	b_1	0.0000
+931	a_1	0.0212
+1132	b_1	0.0000
+1345	a_1	0.0053
+1586	b_1	0.0000
+1802	a_1	0.0012
+2046	b_1	0.0000
+2299	a_1	0.0002
+2561	b_1	0.0000
+2832	a_1	0.0000

[a]Relative to the S_1 C_{2v} minimum.

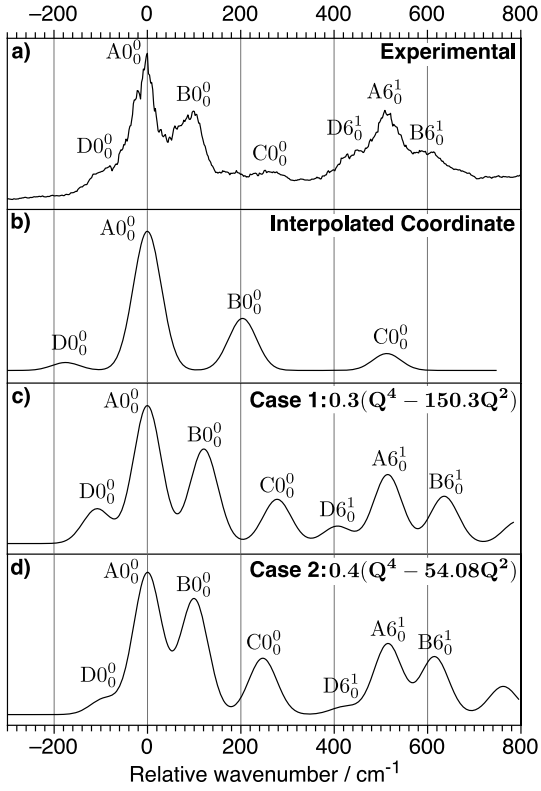

FIG. 10. Comparison between (a) the experimental N_2-tagged PD action spectrum in the vicinity of the electronic origin, (b) the absorption simulation using the CAM-B3LYP/aug-cc-pVDZ interpolated coordinate, and ((c) and (d)) the absorption simulations using the fitted quadratic potential energy surfaces and associated electronic transition dipole moments. The simulated peaks are the convolution of the predicted transitions with 30 cm^{-1} FWHM Gaussians.

reports the predicted transition electric dipole moments and symmetries for transitions into each energy level of the double-well potential from the harmonic ground state. Note that all allowed transitions involve even quanta changes (i.e., they are transitions to symmetric levels).

The single-mode, adiabatic simulation predicts that transitions to the lowest six vibrational levels will have negligible intensity. The transition probability increases sharply about the barrier to planarity (0 cm^{-1}) before decreasing again and levels more than 1000 cm^{-1} higher in energy than the barrier of the double-well potential curve are essentially optically inactive. The most intense spectral feature predicted by this simulation is a $\Delta\tilde{\nu}$ = ~200 cm^{-1} doublet at +53 and +257 cm^{-1}. This is significant as it presents a rationale for closely spaced low-frequency doublet. Additional minor features are predicted 277 cm^{-1} lower in energy and 411 cm^{-1} higher in energy from the centre of the doublet. Fig. 10 compares the first set of four features from the (a) experimental N_2-tagged PD action spectrum, (b) the results of this single-mode simulation convoluted with 40 cm^{-1} full-width half-maximum (FWHM) Gaussian functions, and ((c) and (d)) equivalent simulations performed on mixed quartic/quadratic potential energy functions optimized to reproduce the experimental energy levels, discussed later. The intensity profile is similar for the first four features in the experimental spectrum and the first four significant features in the simulation, however, the absolute energies differ consistently by a factor of two. This double-minimum model provides a rationalization of the low frequency spectral features that are not readily accommodated using vibronic-coupling scenarios that are typically descriptive of aromatic molecular spectroscopy. However, the twofold factor in the energy spacings needs to be addressed. As a check of the calculation, the predicted spacing between the first two a_1 energy levels of the interpolated potential (521 cm^{-1}) should be close to the value of the harmonic TD-DFT frequency of the b_1 nitrogen pyramidalization mode for the non-planar S_1 minimum (530 cm^{-1}). As these two values are similar, 521 cm^{-1} and 530 cm^{-1}, it indicates the two potentials are in close agreement around the non-planar minimum. The nitrogen pyramidalization normal mode for the non-planar S_1 minimum is included in the supplementary material,[65] Sec. 6.3.

The specification of the interpolated coordinate upon which the single point energies in Fig. 7 are calculated is a rudimentary calculation, corresponding to an adiabatic scenario with no simple parameters that can be fitted to the experimental data. Other vibronic coupling and anharmonic interactions not considered here could account for these discrepancies, and would need to be included in a comprehensive simulation. Therefore, it is possible that the method employed above could overestimate the vibrational frequencies by a factor of two. Variations between the interpolated potential energy coordinate in Fig. 8(a) and the actual potential energy curve may also explain the difference between the experimental data and the simulation in Fig. 10(b).

To explore whether the observed spectra features can be explained quantitatively by transitions to vibrational levels supported by a double well potential energy curve, we modelled the potential as a mixed quartic/quadratic function of the form $V = A(Q^4 + BQ^2)$ that was optimized to reproduce the experimental eigenvalues in the Franck-Condon active region about the top of the barrier.[69–71] This was performed in two ways. In the first case (Case 1), the barrier height from the interpolated coordinate was fixed and the equilibrium geometry (i.e., the equilibrium Q value) was unconstrained. The resulting function $V = 0.3(Q^4 - 160.3Q^2)$, plotted in the supplementary material[65] (Fig. S9(a)), exhibits minima at Q = ±8.95 implying either a difference in the mass of the coordinate or a minimum structure that is further displaced from a planar geometry. This quartic potential was used to simulate a Franck-Condon absorption spectrum according to the same formalism used previously. The major features predicted by this model (shown in Fig. 10(c) for the 0_0^0 and 6_0^1 bands) compare well to the observed spectral features. In a second case (Case 2), the equilibrium Q value was fixed at Q = 5.2 (from the interpolated coordinate in Fig. 7) and the barrier height optimized, yielding the function $V = 0.4(Q^4 - 54.08Q^2)$ (supplementary material[65] Fig. S9(b)) with a lowered barrier height of 292 cm^{-1}. The dominant spectral features simulated using this quartic potential are also compared to the experiment shown in Fig. 10(d). Both cases satisfactorily reproduce the experimental spectral features of the PD spectrum in Fig. 10(a). The first four features of the bare ion PD action spectrum compare well to those of the

N_2-tagged species (supplementary material[65] Fig. S10). The assignments presented in Fig. 10 are tabulated with their peak positions in Table S4 in the supplementary material.[65]

It is obvious from Fig. 10 that a mixed quartic/quadratic potential energy function can be used to satisfactorily simulate the main features present in the experimental spectrum and, within this model, the hitherto unassigned features in the *N*-pyridinium electronic spectra can be attributed to the activity of out-of-plane b_1 modes (particularly nitrogen pyramidalization) that are active in the isomerization from a planar excited state structure to a prefulvenic one. A more detailed calculation should include additional vibronic coupling interactions and diabatic electronic states (forgoing the interpolated coordinate).

D. Energy scheme for dissociation

It has been known for more than three decades that the gas-phase *N*-pyridinium ion photodissociates through the loss of molecular hydrogen following ultraviolet irradiation.[32] However, the only other electronic spectrum of which the authors are aware was recorded at low resolution and exhibited no resolved vibronic structure.[32] The spectra reported here exhibit vibronic detail and reflect the bound nature of the excited state. This suggests that the dissociation process may occur on the ground electronic state surface following IC. The spectra where the *N*-pyridinium ion is photodissociated (Fig. 4(b) and Fig. 3) have a more gradual onset than when the ion remains intact (Fig. 4(a)). This suggests that the photodissociation yield increases with photon energy. This can be attributed to either an increase in the IC rate or dissociation of more highly energised ground state ions outcompeting collisional cooling (2.5×10^{-3} Torr Helium $\rightarrow$ $\sim 6 \times 10^4$ collisions·s^{-1}). As discussed in Sec. IV A, in comparison to the d_0 and d_1 spectra, the spectral features in the d_5 spectrum are suppressed at low photon energies. Deuteration is known to greatly decrease the rate of radiationless transitions[72] and it has been shown that skeletal bending and stretching vibrations are important participants in the internal conversion of aromatic nitrogen heterocycles.[73] This observation may be consistent with an IC-mediated process. It is thus reasonable to propose that photodissociation occurs on the vibrationally activated ground electronic state surface following internal conversion.

Benzene is another aromatic compound that can photodissociate in the ultraviolet through the loss of H_2 and this is proposed to occur by a 1,2-hydrogen migration followed by a 1,1-H_2 elimination.[74] *N*-pyridinium is isoelectronic to benzene and an equivalent ground state intramolecular rearrangement was explored for the *N*-pyridinium ion using the CBS-QB3 method. The potential energy diagram for the process is shown in Fig. 11.

The CBS-QB3 method predicts that the initial 1,2-hydrogen migration from the *N*-pyridinium ion occurs through a forward barrier of 72 kcal mol^{-1} to form a structural isomer 60 kcal mol^{-1} higher in energy that is stabilized with respect to the reverse reaction by 12 kcal mol^{-1}. The H_2 dissociation energy is predicted to be 28 kcal mol^{-1} higher in energy than this intermediate and 88 kcal mol^{-1} from the global minimum. No barrier was located for this

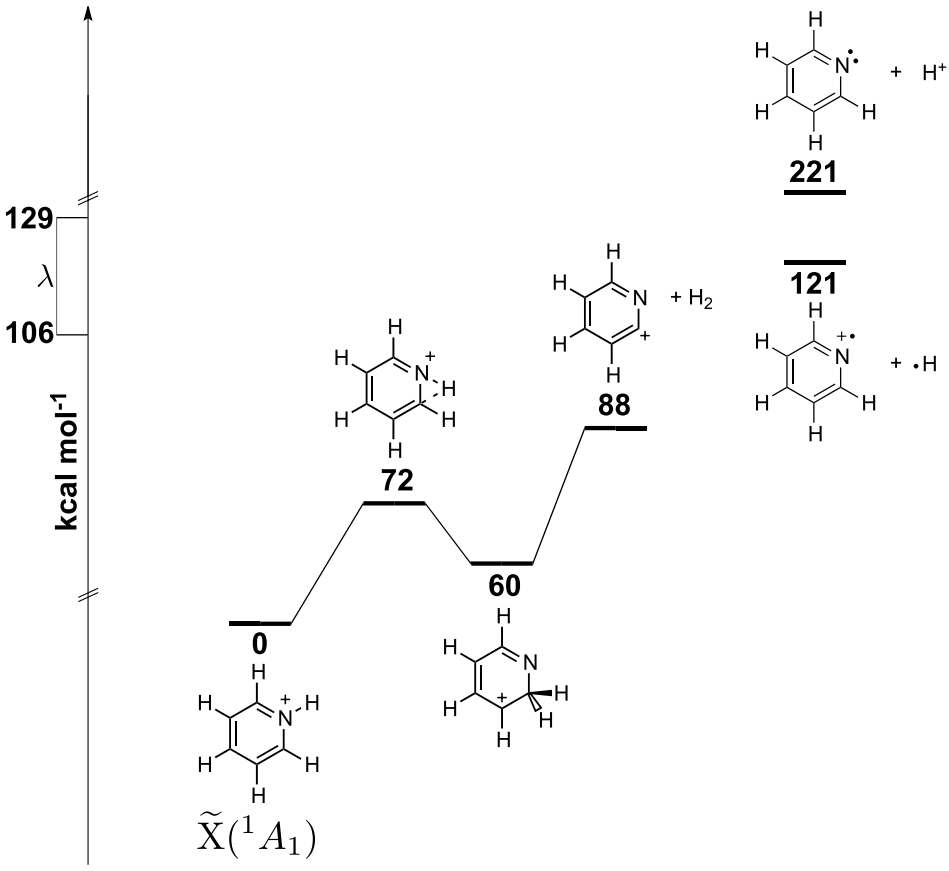

FIG. 11. CBS-QB3 potential energy scheme for the ground-state photodissociation of the *N*-pyridinium ion. The photon energy range spanned by the PD action spectra is labelled on the vertical axis. The energies of the N–H homolysis and heterolysis photoproduct channels are also shown.

final photodissociation process. As mentioned above, the 2-pyridinylium isomer is confirmed to be the exclusive photoproduct channel by structurally diagnostic ion/molecule reaction kinetics (refer to the supplementary material[65] Sec. 3). Production of the unobserved N–H homolysis product is predicted to lie 121 kcal mol^{-1} above the global minimum. The heterolysis/neutralization product, also not observed, is predicted to require 221 kcal mol^{-1} for formation, 92 kcal mol^{-1} above the upper limit of the experimental photon energy range (106–129 kcal mol^{-1}). The potential energy diagram calculated within the same scheme for the d_5 ion is included in the supplementary material,[65] Fig. S11, and predicts a HD dissociation energy of 90 kcal mol^{-1}.

V. CONCLUSION

Photodissociation action spectroscopy in the region 37 000–45 000 cm^{-1} (270–220 nm) was used to characterize the electronic spectrum of the *N*-pyridinium ion. Experiments were performed on both ambient-temperature bare ions and cooler N_2-tagged ions using two different instrumental arrangements. It was found that, following ultraviolet irradiation, *N*-pyridinium photodissociates through the loss of molecular hydrogen, H_2, to form exclusively the 2-pyridinylium ion, a result confirmed by structurally diagnostic ion/molecule reaction kinetics. This dissociation is rationalized as proceeding on the ground state electronic surface following internal conversion. The first vibronically resolved, gas-phase electronic spectra are reported for the *N*-pyridinium ion and its $C_5H_5ND^+$ and $C_5D_5NH^+$ isotopologues. It was found that the ground electronic state is planar while the excited state adopts a significantly ring-buckled geometry. The vibronic detail in the electronic spectra is attributed to even quanta transitions of out-of-plane b_1 normal modes that are active in this deformation and add to progressions in two totally symmetric ring-deformation modes that are built off a weak origin arising from the non-planar minimum and consequent breakdown of the Condon approximation.

ACKNOWLEDGMENTS

This project was supported financially by the following Australian Research Council (ARC) Grant Nos. S.J.B. and A.J.T.: CE0561607, DP1094135, DP140101237. E.J.B.: DP110100312, DP120100100. J.R.R.: DP110102932. The authors are grateful to the Intersect Resource Allocation Committee and the National Computational Infrastructure (NCI) Merit Allocation Scheme (MAS) for awards of super computing time on the NCI National Facility (ACT, Australia).

[1]A. V. Bochenkova and L. H. Andersen, Faraday Discuss. **163**, 297 (2013).
[2]D. Picconi, F. J. A. Ferrer, R. Improta, A. Lami, and F. Santoro, Faraday Discuss. **163**, 223 (2013).
[3]A. L. Sobolewski, W. Domcke, C. Dedonder-Lardeux, and C. Jouvet, Phys. Chem. Chem. Phys. **4**, 1093 (2002).
[4]M. N. R. Ashfold, B. Cronin, A. L. Devine, R. N. Dixon, and M. G. D. Nix, Science **312**, 1637 (2006).
[5]G. M. Roberts, C. A. Williams, H. Yu, A. S. Chatterley, J. D. Young, S. Ullrich, and V. G. Stavros, Faraday Discuss. **163**, 95 (2013).
[6]T. Gustavsson, R. Improta, and D. Markovitsi, J. Phys. Chem. Lett. **1**, 2025 (2010).
[7]D. Murdock, S. J. Harris, T. N. V. Karsili, G. M. Greetham, I. P. Clark, M. Towrie, A. J. Orr-Ewing, and M. N. R. Ashfold, J. Phys. Chem. Lett. **3**, 3715 (2012).
[8]J. R. Reimers and Z.-L. Cai, Phys. Chem. Chem. Phys. **14**, 8791 (2012).
[9]A. Tielens, Annu. Rev. Astron. Astrophys. **46**, 289 (2008).
[10]V. Dryza, J. A. Sanelli, E. G. Robertson, and E. J. Bieske, J. Phys. Chem. A **116**, 4323 (2012).
[11]P. G. Stoks and A. W. Schwartz, Geochim. Cosmochim. Acta **46**, 309 (1982).
[12]P. G. Stoks and A. W. Schwartz, Geochim. Cosmochim. Acta **44**, 563 (1981).
[13]A. Somogyi, C.-H. Oh, M. A. Smith, and J. I. Lunine, J. Am. Soc. Mass Spectrom. **16**, 850 (2005).
[14]S. Soorkia, C. A. Taatjes, D. L. Osborn, T. M. Selby, A. J. Trevitt, K. R. Wilson, and S. R. Leone, Phys. Chem. Chem. Phys. **12**, 8750 (2010).
[15]Z. Peeters, O. Botta, S. B. Charnley, Z. Kisiel, Y.-J. Kuan, and P. Ehrenfreund, Astron. Astrophys. **433**, 583 (2005).
[16]Z. Cai and J. Reimers, J. Phys. Chem. A **104**, 8389 (2000).
[17]M. Chachisvilis and A. Zewail, J. Phys. Chem. A **103**, 7408 (1999).
[18]J. Martin and C. VanAlsenoy, J. Phys. Chem. **100**, 6973 (1996).
[19]K. Innes, I. Ross, and W. Moomaw, J. Mol. Spectrosc. **132**, 492 (1988).
[20]M. Rosenberg, C. Dahlstrand, K. Kilsa, and H. Ottoson, Chem. Rev. **114**, 5379 (2014).
[21]I. Palmer, I. Ragazos, F. Bernadi, M. Olivucci, and M. Robb, J. Am. Chem. Soc. **115**, 673 (1993).
[22]A. Sobolewski, C. Woywod, and W. Domcke, J. Chem. Phys **98**, 5627 (1993).
[23]D. Zhong, E. W.-G. Diau, T. M. Bernhardt, S. D. Feyter, J. D. Roberts, and A. H. Zewail, Chem. Phys. Lett. **298**, 129 (1998).
[24]A. Sobolewski and W. Domcke, Chem. Phys. Lett. **180**, 381 (1991).
[25]K. Grove, R. A. King, and U. Burger, J. Mol. Struct.: THEOCHEM **807**, 25 (2007).
[26]D. E. Johnstone and J. R. Sodeau, J. Phys. Chem. **95**, 165 (1991).
[27]K. E. Wilzbach and D. J. Rausch, J. Am. Chem. Soc. **92**, 2178 (1970).
[28]T. Damiano, D. Morton, and A. Nelson, Org. Biomol. Chem. **5**, 2735 (2007).
[29]I. Yamazaki and H. Baba, J. Chem. Phys. **66**, 5826 (1977).
[30]I. Yamazaki, K. Sushida, and H. Baba, J. Chem. Phys. **71**, 381 (1979).
[31]S. Nagaoka and U. Nagashima, J. Phys. Chem. **94**, 4467 (1990).
[32]B. Freiser and J. Beauchamp, J. Am. Chem. Soc. **99**, 3214 (1977).
[33]J. I. Selco, P. L. Holt, and R. B. Weisman, J. Chem. Phys. **79**, 3269 (1983).
[34]C. S. Hansen, B. B. Kirk, S. J. Blanksby, R. A. J. O'Hair, and A. J. Trevitt, J. Am. Soc. Mass Spectrom. **24**, 932 (2013).
[35]D. Wild and E. Bieske, Int. Rev. Phys. Chem. **22**, 129 (2003).
[36]D. G. Harman and S. J. Blanksby, Org. Biomol. Chem. **5**, 3495 (2007).
[37]N. Yamamoto, T. Vreven, M. Robb, M. Frisch, and H. Schlegel, Chem. Phys. Lett. **250**, 373 (1996).
[38]M. Frisch, I. Ragazos, M. Robb, and H. Schlegel, Chem. Phys. Lett. **189**, 524 (1992).
[39]F. Bernardi, A. Bottoni, J. McDouall, M. Robb, and H. Schlegel, Faraday Symp. Chem. Soc. **19**, 137 (1984).
[40]H. Schlegel and M. Robb, Chem. Phys. Lett. **93**, 43 (1982).
[41]R. Eade and M. Robb, Chem. Phys. Lett. **83**, 362 (1981).
[42]D. Hegarty and M. Robb, Mol. Phys. **38**, 1795 (1979).
[43]M. J. Frisch, G. W. Trucks, H. B. Schlegel, G. E. Scuseria, M. A. Robb, J. R. Cheeseman, G. Scalmani, V. Barone, B. Mennucci, G. A. Petersson, H. Nakatsuji, M. Caricato, X. Li, H. P. Hratchian, A. F. Izmaylov, J. Bloino, G. Zheng, J. L. Sonnenberg, M. Hada, M. Ehara, K. Toyota, R. Fukuda, J. Hasegawa, M. Ishida, T. Nakajima, Y. Honda, O. Kitao, H. Nakai, T. Vreven, J. A. Montgomery, Jr., J. E. Peralta, F. Ogliaro, M. Bearpark, J. J. Heyd, E. Brothers, K. N. Kudin, V. N. Staroverov, R. Kobayashi, J. Normand, K. Raghavachari, A. Rendell, J. C. Burant, S. S. Iyengar, J. Tomasi, M. Cossi, N. Rega, M. J. Millam, M. Klene, J. E. Knox, J. B. Cross, V. Bakken, C. Adamo, J. Jaramillo, R. Gomperts, R. E. Stratmann, O. Yazyev, A. J. Austin, R. Cammi, C. Pomelli, J. W. Ochterski, R. L. Martin, K. Morokuma, V. G. Zakrzewski, G. A. Voth, P. Salvador, J. J. Dannenberg, S. Dapprich, A. D. Daniels, Ö. Farkas, J. B. Foresman, J. V. Ortiz, J. Cioslowski, and D. J. Fox, GAUSSIAN 09, Revision C.01, Gaussian Inc., Wallingford, CT, 2009.
[44]T. Dunning, J. Chem. Phys. **90**, 1007 (1989).
[45]D. Woon and T. Dunning, J. Chem. Phys. **98**, 1358 (1993).
[46]R. Kendall, T. Dunning, and R. Harrison, J. Chem. Phys. **96**, 6796 (1992).
[47]C. M. Western, PGOPHER, a program for simulating rotational structure, University of Bristol, 2010, http://pgopher.chm.bris.ac.uk.

[48]G. Scalmani, M. Frisch, B. Mennucci, J. Tomasi, R. Cammi, and V. Barone, J. Chem. Phys. **124**, 094107 (2006).
[49]F. Furche and R. Ahlrichs, J. Chem. Phys. **117**, 7433 (2002).
[50]C. Van Caillie and R. Amos, Chem. Phys. Lett. **317**, 159 (2000).
[51]C. Van Caillie and R. Amos, Chem. Phys. Lett. **308**, 249 (1999).
[52]R. Stratmann, G. Scuseria, and M. Frisch, J. Chem. Phys. **109**, 8218 (1998).
[53]M. Casida, C. Jamorski, K. Casida, and D. Salahub, J. Chem. Phys. **108**, 4439 (1998).
[54]R. Bauernschmitt and R. Ahlrichs, Chem. Phys. Lett. **256**, 454 (1996).
[55]T. Yanai, D. Tew, and N. Handy, Chem. Phys. Lett. **393**, 51 (2004).
[56]J. Reimers, J. Chem. Phys **115**, 9103 (2001).
[57]J. Montgomery, M. Frisch, J. Ochterski, and G. Petersson, J. Chem. Phys. **112**, 6532 (2000).
[58]J. Montgomery, M. Frisch, J. Ochterski, and G. Petersson, J. Chem. Phys. **110**, 2822 (1999).
[59]J. Ochterski, G. Petersson, and J. Montgomery, J. Chem. Phys. **104**, 2598 (1996).
[60]J. Montgomery, J. Ochterski, and G. Petersson, J. Chem. Phys. **101**, 5900 (1994).
[61]G. Petersson and M. Allaham, J. Chem. Phys. **94**, 6081 (1991).
[62]G. Petersson, T. Tensfeldt, and J. Montgomery, J. Chem. Phys. **94**, 6091 (1991).
[63]G. Petersson, A. Bennett, T. Tensfeldt, M. Allaham, W. Shirley, and J. Mantzaris, J. Chem. Phys. **89**, 2193 (1988).
[64]M. Nyden and G. Petersson, J. Chem. Phys. **75**, 1843 (1981).
[65]See supplementary material at http://dx.doi.org/10.1063/1.4904267 for additional information as referred to in the text: including description of normal modes and geometries, the d_5 PD action spectrum, structurally-diagnostic ion/molecule kinetics, comparison with spectra acquired using a narrow-linewidth dye laser and further details/results from the computational analysis.
[66]D. Norberg, P.-E. Larsson, and N. Salhi-Benachenhou, J. Phys. Chem. A **112**, 4694 (2008).
[67]C. S. Hansen, B. B. Kirk, S. J. Blanksby, and A. J. Trevitt, J. Phys. Chem. A **117**, 10839 (2013).
[68]D. Harris and M. Bertolucci, *An Introduction to Vibrational and Electronic Spectroscopy* (Oxford University Press, New York, 1978).
[69]J. Laane, Int. Rev. Phys. Chem. **18**, 301 (1999).
[70]H. -L. Sheu, S. Kim, and J. Laane, J. Phys. Chem. A **117**, 13596 (2013).
[71]J. Laane, J. Phys. Chem. A **104**, 7715 (2000).
[72]M. Bixon and J. Jortner, J. Chem. Phys. **48**, 715 (1968).
[73]J. Byrne, E. McCoy, and I. Ross, Aust. J. Chem. **18**, 1589 (1965).
[74]V. Kislov, T. Nguyen, A. Mebel, S. Lin, and S. Smith, J. Chem. Phys. **120**, 7008 (2004).